第 33 卷第 3 期
2014 年 6 月

红 外 与 毫 米 波 学 报
J. Infrared Millim. Waves

Vol. 33, No. 3
June, 2014

文章编号:1001 - 9014(2014)03 - 0213 - 05

DOI:10.3724/SP. J. 1010. 2014. 00213

InAs/InGaAs digital alloy strain-compensated quantum well lasers

CAO Yuan-Ying, GU Yi, ZHANG Yong-Gang*, LI Yao-Yao, FANG Xiang, LI Ai-Zhen, ZHOU Li, LI Hao-Si-Bai-Yin

(State Key Laboratory of Functional Materials for Informatics, Shanghai Institute of Microsystem and Information Technology, Chinese Academy of Sciences, Shanghai 200050, China)

Abstract: InAs/InGaAs digital alloy strain-compensated quantum well lasers have been grown on InP substrate by gas source molecular beam epitaxy. Multiple quantum wells composed of compressive InAs/$In_{0.53}Ga_{0.47}As$ digital alloy triangular wells and tensile $In_{0.43}Ga_{0.57}As$ barriers were used as the active region. X-ray diffraction measurements confirmed the pseudomorphic growth and high crystalline quality of the QW structures. The peak emission wavelength of the laser is 1.94 μm at 100 K under continuous-wave driving current of 130 mA, and the threshold current density is 2.58 kA/cm^2. An unusual blue shift of the laser spectral with the increase of the temperature was found, which is originated from the reduced slope of maximum gain function, due to the relatively high internal absorption and weak optical confinement in the laser structure.

Key words: digital alloy, quantum well, molecular beam epitaxy
PACS: 61.05.cp, 78.67.De, 81.05.Ea, 81.15.Hi

InAs/InGaAs 数字合金应变补偿量子阱激光器

曹远迎, 顾 溢, 张永刚*, 李耀耀, 方 祥, 李爱珍, 周 立, 李好斯白音
(中国科学院上海微系统与信息技术研究所 信息功能材料国家重点实验室,上海 200050)

摘要:采用气态源分子束外延在InP衬底上生长InAs/InGaAs数字合金应变补偿量子阱激光器.有源区的多量子阱结构由压应变的InAs/$In_{0.53}Ga_{0.47}As$数字合金三角形势阱和张应变的$In_{0.43}Ga_{0.57}As$势垒构成.X射线衍射测试表明赝晶生长的量子阱结构具有很高的晶格质量.在100 K、130 mA连续波工作模式下,激光器的峰值波长达到1.94 μm,对应的阈值电流密度为2.58 kA/cm^2.随着温度升高,激光器的激射光谱出现独特的蓝移现象,这是由于激光器结构中相对较高的内部吸收和弱的光学限制引起最大增益函数斜率降低所导致的.

关 键 词:数字合金;量子阱;分子束外延
中图分类号:TN2 **文献标识码**:A

Introduction

Semiconductor lasers emitting around 2 μm have attracted much attention due to their applications in molecular spectroscopy and trace-gas sensing[1-2]. Strong absorption lines of various gases such as carbon monoxide (CO) and carbon dioxide (CO_2) are located in this wavelength range. Traditionally such semiconductor lasers are developed in InGaAsSb/ AlGaAsSb material system on GaSb substrate[3-5]. $In_xGa_{1-x}As/In_{0.53}Ga_{0.47}As$ ($x>0.53$) quantum well (QW) laser on InP substrate is another approach in this spectral range owing to the superior quality of InP substrate as well as the mature growth and processing technology[6-9]. The emission wavelength can be tailored by adjusting the indium composition of InGaAs QWs, whereas it is really a challenge to extend the wavelength much longer due to the large lattice mismatch and strain in the QW[10-11]. In our previous work, the emission wavelength of the InAs/InGaAs strained

Received date: 2013 - 04 - 08, **revised date**: 2014 - 03 - 11 **收稿日期**:2013 - 04 - 08, **修回日期**:2014 - 03 - 11
Foundation items:Supported by National Basic Research Program of China (2012CB619200), National Natural Science Foundation of China (61275113 and 61204133)
Biography:CAO Yuan-Ying(1986-), male, Shanghai, Ph. D. candidate. Research area is optoelectronic materials and devices. E-mail: yycao@mail.sim.ac.cn
* **Corresponding author**:E-mail: ygzhang@mail.sim.ac.cn

QWs can be increased effectively by changing the band shape in the wells from conventional rectangular to triangular one, while keeping the same strain content[12]. In this case the indium composition in the well layers is varied from 0.53 to 1, and then to 0.53 again. A novel growth process of digital alloy (DA) technology, which simulates desired compound alloy compositions by growing short period superlattices of two defined compositions at certain digital thickness ratio, can be applied to approximate the triangular shape of QWs effectively using molecular beam epitaxy[13]. In this letter, InAs/InGaAs quantum well lasers on InP substrate have been demonstrated, where symmetrical triangular QWs composed of compressive InAs/$In_{0.53}Ga_{0.47}As$ DA triangular wells and tensile $In_{0.43}Ga_{0.57}As$ barriers are used as the active region. The growth procedure, material structural properties and laser performances are analyzed in detail.

1 Experimental details

The samples were grown on (100) InP epi-ready substrates by using a VG Semicon V80H gas source molecular beam epitaxy (GSMBE) system. The elemental indium and gallium dual filament thermo-cells were used as group Ⅲ sources, and their fluxes were controlled by changing the cell temperatures during growth. Arsine (AsH_3) and phosphine (PH_3) were cracked to form As_2 and P_2 at 1 000 ℃ as group V sources, and their fluxes were controlled by adjusting the pressure. Standard beryllium (Be) and silicon (Si) effusion cells were used as p-and n-type doping sources, and the doping levels were also controlled by changing the cell temperatures. Prior to the growth, reflection high energy electron diffraction (RHEED) was used to determine the surface oxide desorption of InP substrate under P_2 flux. This involved a slow ramp-up of the substrate temperature until the pattern showed an abrupt transformation to 2×4 surface reconstruction. The substrate desorption temperature was 470 ℃ measured by thermocouple, while the growth temperature was 420 ℃ and 460 ℃ for InP and In(Ga)As, respectively.

The layer parameters of the laser structures are listed in Table 1. The growth sequence started with a 1 000-nm-thick n-type InP cladding layer (Si, 2×10^{18} cm^{-3}). Then a 150-nm-thick n-type InP waveguide layer (Si, 5×10^{17} cm^{-3}) was grown. The following active QW region was formed by two periods of triangular QWs. Each period was composed of a 12-nm-thick compressive InAs/$In_{0.53}Ga_{0.47}As$ triangular QW sandwiched by tensile $In_{0.43}Ga_{0.57}As$ barriers. The well layers were grown by digital alloy technology and composed of digital graded InAs/$In_{0.53}Ga_{0.47}As$ ultra-thin layers[14] while the $In_{0.43}Ga_{0.57}As$ barrier layers were grown by random alloy technology using another indium cell. After that a 150-nm-thick p-type InP upper waveguide layer (Be, 5×10^{17} cm^{-3}) and a 50-nm-thick p-type $In_{0.53}Ga_{0.47}As$ etch stop layer (Be, 5×10^{18} cm^{-3}) were deposited. Subsequently a 500-nm-thick p-type (Be, 5×10^{18} cm^{-3}) and a 1 200-nm-thick highly doped p-type (Be, 1×10^{19} cm^{-3}) InP cladding layers were grown. Finally a 300-nm-thick highly doped p-type $In_{0.53}Ga_{0.47}As$ cap layer (Be, 1×10^{19} cm^{-3}) was grown. The schematic energy-band of the active zone is shown in Fig. 1.

Table 1 Layer parameters of the QW laser structure
表1 量子阱激光器的材料结构参数

Layer	Material	Thickness(nm)	Concentration(cm^{-3})
Cap	$In_{0.53}Ga_{0.47}As$: Be	300	$p=1\times10^{19}$
Cladding	InP: Be	1 200	$p=1\times10^{19}$
Cladding	InP: Be	500	$p=5\times10^{18}$
Etch stop	$In_{0.53}Ga_{0.47}As$: Be	50	$p=5\times10^{18}$
Waveguide	InP: Be	150	$p=5\times10^{17}$
Barrier	$In_{0.43}Ga_{0.57}As$	12	Undoped
Triangular well	InAs/$In_{0.53}Ga_{0.47}As$	12	Undoped
Barrier	$In_{0.43}Ga_{0.57}As$	24	Undoped
Triangular well	InAs/$In_{0.53}Ga_{0.47}As$	12	Undoped
Barrier	$In_{0.43}Ga_{0.57}As$	12	Undoped
Waveguide	InP: Si	150	$n=5\times10^{17}$
Cladding	InP: Si	1 000	$n=2\times10^{18}$
Substrate	InP: S	350 μm	$n=2\times10^{17}$

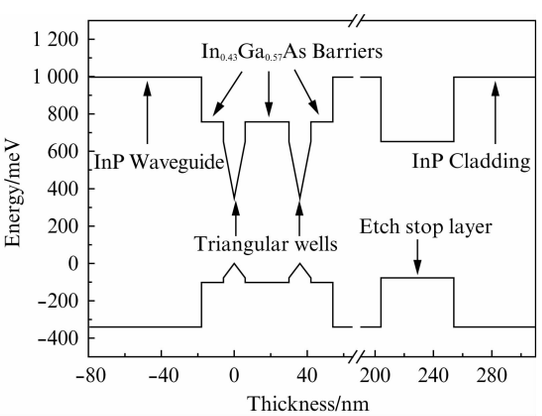

Fig. 1 Schematic energy-band diagram of the active zone
图1 有源区的能带示意图

After growth, the structural properties of the QW parts were characterized by using high resolution X-ray diffraction (HRXRD) measurements after etching away the cap and cladding layers, where a Philips X'pert X-ray diffractometer equipped with a four-crystal Ge (220) monochromator was applied. Ridge waveguide structures with strip width of 6 μm were fabricated by standard lithography and wet chemical etching process. Then a 300-nm-thick Si_3N_4 layer was deposited by plasma enhanced chemical vapor deposition (PECVD) as insulator. After that, a 4-μm-wide window was patterned on top of the ridge. Ti/Pt/Au was sputtered as a top metallic contact, then the samples were thinned to 100-120 μm and Ge/Au/Ni/Au was evaporated on the back of the substrate as a back metallic contact. The chips were cleaved into 0.8-mm-long bars with the facet uncoated, soldered on copper heat sinks and wire bonded. The spectral features of the laser were characterized by using a Nicolet 860 Fourier transform infrared (FTIR) spectrometer with liquid-nitrogen cooled InSb detector and CaF_2 beam splitter. The current-power (I-P) and cur-

rent-voltage (I-V) characteristics of the laser under continuous-wave (CW) driving conditions were measured by a Keithley 2 420 source meter and a Coherent EMP1000 power meter with PS19 thermopile detector. The heat sink temperature of the laser was controlled by using an Oxford Optistat DN-V variable temperature liquid nitrogen cryostat.

2 Results and discussions

The HRXRD (004) ω/2θ scan curves of the QW structures are shown in Fig. 2. The upper one was the measured curve and the lower one was the simulated curve. The measured curve of the sample showed multiple satellite peaks on both sides of the substrate peak, indicating that strain relaxation did not occur in the QWs. The signal envelops on the left and right sides of the substrate peak were related to compressive InAs/$In_{0.53}Ga_{0.47}As$ triangular wells and tensile $In_{0.43}Ga_{0.57}As$ barriers, respectively. The significant compressive strain in the QWs was partially compensated by the tensile barriers but not overcompensated. It also can be seen that the positions of satellite peaks in the measured curve matched well with the simulation. The results give the evidence of pseudomorphic growth and indicate the high crystalline quality of the QW structures.

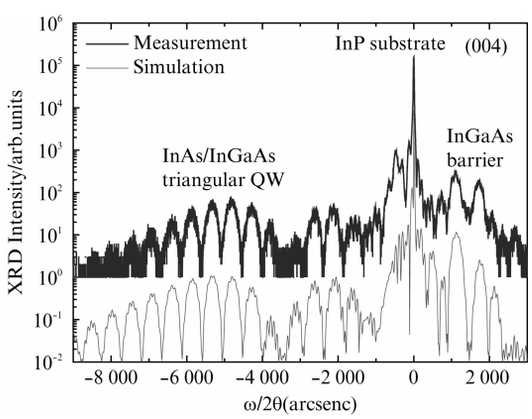

Fig. 2　Measured (upper) and simulated (lower) HRXRD rocking curves of the QW structure
图 2　测试(上)和模拟(下)的量子阱结构的 X 射线衍射摇摆曲线

The spectral characteristics and tunability of the lasers were measured by using the FTIR spectrometer with resolution of 0.125 cm^{-1}. Figure 3 shows the lasing spectra of a 6-μm-wide and 800-μm-long laser at temperature from 99 K to 107 K in step of 2 K. The laser was operated at a driving current of 250 mA in pulsed mode with a pulse width of 500 ns and a repetition frequency of 100 kHz. It can be seen that the lasing wavelength blue shifted from 1.940 μm at 99 K to 1.926 μm at 107 K. The unusual blue shift of the laser spectra with the increase of the temperature may be resulted from the reduced slope of maximum gain function $G(E)$, due to the relatively high internal absorption and weak optical confinement in the laser structure[15]. It is well known that the material gain g_{mat} is correlated with the modal gain g_{mod} via

$$g_{mod} = g_{mat} \times \Gamma - \alpha_i(T) \quad , \quad (1)$$

where Γ is the optical confinement factor and α_i is the internal absorption. By increasing the carrier density and thus the Fermi level, the energetic position of the gain maximum shifts towards higher energies. Therefore the curve described by the point of maximum modal gain is called the "maximum modal gain function" $G(E)$. Generally, the internal absorption α_i increases as the operation temperature T increases in semiconductor lasers, which is mainly due to an increased amount of free carrier absorption. Therefore, the modal gain g_{mod} will reduce as the temperature increases as shown in literature[15]. Besides, in this laser structure the waveguide and the cladding layers are both InP as shown in Fig. 1, the optical confinement factor Γ is about 0.24 by calculation, which is relatively weak. Consequently, with the temperature increased, the necessary modal gain for a given laser geometry can only be obtained closer to the transition between the first excited electron and hole states which results in an inevitable blue shift of the laser line relative to the gain spectrum of the laser. It is also obvious that the slope of the maximum modal gain function $G(E)$ determines the magnitude of the relative blue shift.

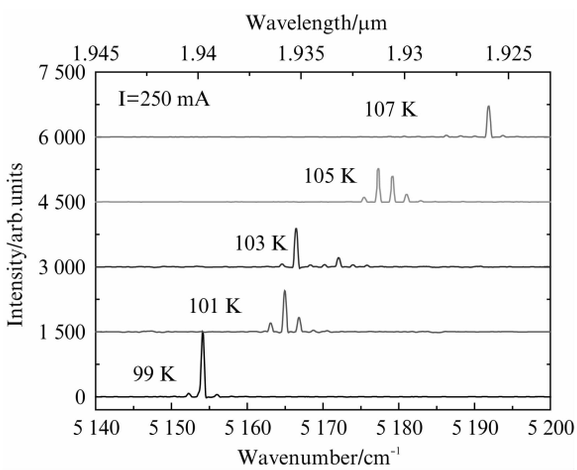

Fig. 3　Lasing spectra of the laser at temperature from 99 K to 107 K in step of 2 K
图 3　在 99 K 到 107 K 的温度区内,每间隔 2 K 测得的激光器的激射光谱

To investigate the temperature-dependent spectral characteristics and tunability more clearly, the lasing spectra of the same laser was investigated under the same driving current at a smaller temperature step of 0.5 K from 101 K to 103 K as shown in Fig. 4. It can be seen that, as temperature increased from 101 K to 103 K, the lower energy lasing mode (mode 1) red shifted continuously from 1936.084 nm to 1936.210 nm and the higher energy lasing mode (mode 2) red shifted continuously from 1935.366 nm to 1935.509 nm, respectively. For the same lasing mode, the average wavelength shift as a function of temperature Δλ/ΔT was about 0.067 nm/K, which could be attributed to the refractive index change with the temperature. In addition, as the temperature increases, the lasing intensity of mode 2 increases, whereas the intensity of mode 1 decreases, which formed the temperature-dependent spectral characteristics as shown in Fig. 3.

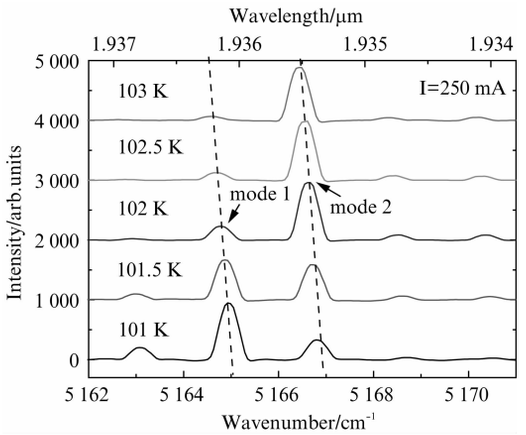

Fig. 4 Lasing spectra of the laser at temperature from 103 K to 103 K in step of 0.5 K

图4 在101 K到103 K的温度区间内,每间隔0.5 K测得的激光器的激射光谱

The laser characteristics under CW driving condition have also been measured as shown in Fig. 5. The peak emission wavelength was 1.942 μm at an injection current of 130 mA at 100 K. Figure 6 shows I-P and *I-V* characteristics of the laser under CW driving conditions from 80 K to 105 K. At 100 K, the threshold current was 124 mA, corresponding to a threshold current density of 2.58 kA/cm^2. The turn-on voltage of the laser was about 1 V and a differential resistance of about 5.4 Ω was obtained.

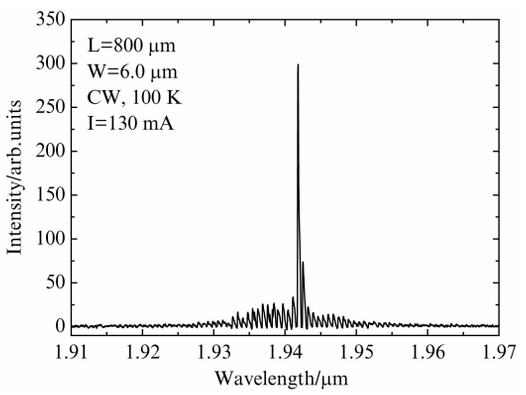

Fig. 5 Lasing spectra of the laser under CW driving condition at 100 K

图5 温度100 K,连续波工作模式下激光器的激射光谱

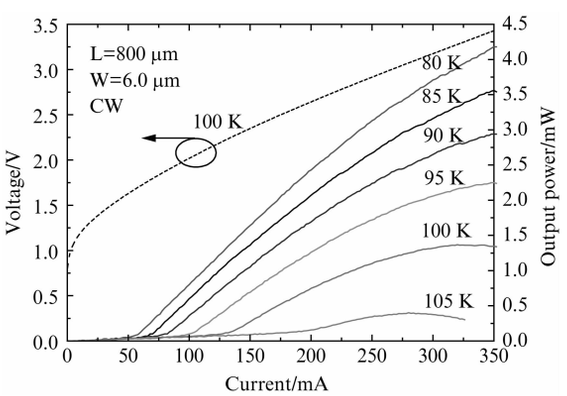

Fig. 6 *I-P* and *I-V* characteristics of the laser under CW driving conditions

图6 连续波工作模式下,激光器的电流-功率和电流-电压特性

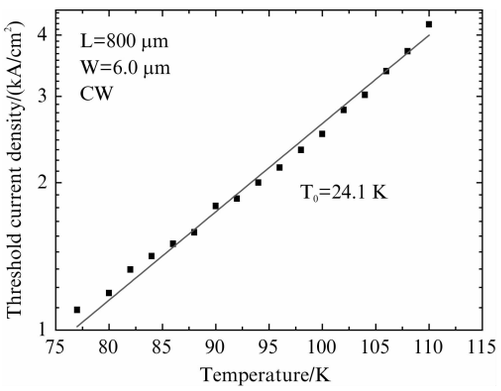

Fig. 7 Characteristic temperature dependence of threshold current density for the laser under CW driving conditions

图7 连续波工作模式下,激光器阈值电流密度的温度特性

The temperature dependence of threshold current density for the laser under CW driving conditions is shown in Fig. 7. By fitting J_{th} data, a characteristic temperature of T_0 = 24.1 K was obtained in the 77 K to 110 K temperature range. This T_0 is relatively lower than the values reported in other publications for InP based 2 μm strained QW lasers, where the typical T_0 values are about 30 ~ 50 K.[16-18] A possible reason may be that in this laser the waveguide and cladding layers use the same InP materials, which causes relatively weak optical confinement, and thus a relatively lower T_0. In the further device demonstration, the optical confinement still needs to be improved.

3 Conclusions

In conclusion, InP-based InAs/InGaAs compressively strained quantum well lasers emitting at 2 μm have been grown by GSMBE. A symmetrical triangular QW structure composed of InAs/ $In_{0.53}Ga_{0.47}As$ DA triangular well and tensile $In_{0.43}Ga_{0.57}As$ barrier is used as the active region. The pseudomorphic growth and high crystalline quality of the QW structures have been confirmed by the HRXRD measurements. The unusual blue shift of the laser spectral with the increase of the temperature may be resulted from the reduced slope of maximum gain function $G(E)$ and the little red shift of the same mode can be attributed to the change of refractive index with the temperature. At 100 K, the laser has a threshold current density of 2.58 kA/cm^2 and emits at 1.94 μm under CW driving current of 130 mA. A characteristic temperature of 24.1 K in 77 ~ 110 K range under CW driving conditions has also been measured.

References

[1] Mattiello M, Niklès M, Schilt S, *et al*. Novel Helmholtz-based photoacoustic sensor for trace gas detection at ppm level using GaInAsSb/GaAlAsSb DFB lasers[J]. *Spectrochimica Acta Part A*, 2006, **63**: 952 - 958.

[2] Jean B, Bende T. Mid-IR laser applications in medicine[J]. *Topics In Applied Physics*, 2003, **89**: 511 - 544.

[3] Kim J G, Shterengas L, Martinelli R U, *et al*. Room-temperature 2.5 μm InGaAsSb/AlGaAsSb diode lasers emitting 1 W continuous waves[J]. *Applied Physics Letters*, 2002, **81**(17): 3146 - 3148.

[4] Zhang Y G, Zheng Y L, Lin C, *et al*. Continuous wave performance and tenability of MBE grown 2.1 μm InGaAsSb/AlGaAsSb MQW lasers[J]. *Chinese Physics Letters*, 2006,**23**(8): 2262-2265.

[5] O'Brien K, Sweeney S J, Adams A R, *et al*. Recombination processes in midinfrared InGaAsSb diode lasers emitting at 2.37 μm[J]. *Applied Physics Letters*, 2006,**89**(5): 051104.

[6] Forouhar S, Ksebdzov A, Larsson A, *et al*. InGaAs/lnGaAsP/lnP Strained-layer quantum well lasers at 2 μm[J]. *Electronics Letters*, 1992,**28**(15): 1431-1432.

[7] Mitsuhara M, Ogasawara M, Oishi M, *et al*. Metalorganic molecular-beam-epitaxy-grown $In_{0.77}Ga_{0.23}As$/InGaAs multiple quantum well lasers emitting at 2.07 μm wavelength[J]. *Applied Physics Letters*, 1998,**72**(24): 3106-3108.

[8] Serries D, Peter M, Kiefer R, *et al*. Improved Performance of 2-μm GaInAs Strained Quantum-Well Lasers on InP by Increasing Carrier Confinement[J]. *IEEE Photonics Technology Letters*, 2001,**13**(5): 412-414.

[9] Sato T, Mitsuhara M, Watanabe T, *et al*. Surfactant-mediated growth of InGaAs multiple-quantum-well lasers emitting at 2.1 μm by metalorganic vapor phase epitaxy[J]. *Applied Physics Letters*, 2005,**87**(21): 211903.

[10] Zheng L, Lin C H, Singer K E, *et al*. Strained GaInAs quantum well mid-IR emitters[J]. *IEE Proc.-Optoelectron*, 1997,**144**(5): 360-364.

[11] Sato T, Mitsuhara M, Nunoya N, *et al*. 2.33-μm-Wavelength Distributed Feedback Lasers With InAs-$In_{0.53}Ga_{0.47}As$ Multiple-Quantum Wells on InP Substrates[J]. *IEEE Photonics Technology Letters*, 2008,**20**(12): 1045-1047.

[12] Gu Y, Zhang Y G, Liu S, *et al*. Strain Compensated AlInGaAs/InGaAs/InAs Triangular Quantum Wells for Lasing Wavelength beyond 2 μm[J]. *Chinese Physics Letters*, 2007,**24**(11): 3237-3240.

[13] Mourad C, Gianardi D, Malloy K J, *et al*. 2 μm GaInAsSb/AlGaAsSb midinfrared laser grown digitally on GaSb by modulated-molecular beam epitaxy[J]. *Journal of Appiled Physics*, 2000,**88**(10): 5543-5546.

[14] Gu Y, Zhang Y G, Wang K, *et al*. AlInGaAs/InGaAs/InAs strain compensated triangular quantum wells grown by gas source molecular beam epitaxy for laser applications in 2.1-2.4 μm range[J]. *Journal of Crystal Growth*, 2009,**311**:1935-1938.

[15] Klopf F, Deubert S, Reithmaier J P, *et al*. Correlation between the gain profile and the temperature-induced shift in wavelength of quantum-dot lasers[J]. *Applied Physics Letters*, 2002,**81**(2): 217-219.

[16] Ochiai M, Temkin H, Forouhar S, *et al*. InGaAs-InGaAsP Buried Heterostructure Lasers Operating at 2.0 μm[J]. *IEEE Photonics Technology Letters*, 1995,**7**(8): 825-827.

[17] Dong J, Ubukata A, Matsumoto K. Characteristics Dependence on Confinement Structure and Single-Mode Operation in 2-μm Compressively Strained InGaAs-InGaAsP Quantum-Well Lasers[J]. *IEEE Photonics Technology Letters*, 1998,**10**(4): 513-515.

[18] Mitsuhara M, Ogasawara M, Oishi M, *et al*. 2.05-μm Wavelength InGaAs-InGaAs Distributed-Feedback Multiquantum-Well Lasers with 10-mW Output Power[J]. *IEEE Photonics Technology Letters*, 1999, **11**(1): 33-35.